Development and characterization of low emitting ceramics

J. Manara[1], M. Reidinger, S. Korder, M. Arduini-Schuster, J. Fricke
Bayerisches Zentrum für Angewandte Energieforschung e.V. (ZAE Bayern)
Am Hubland, D-97074 Würzburg, Germany
[1]   To whom correspondence should be adressed:
       email: manara@zae.uni-wuerzburg.de
       Tel.: +49-931-70564-46, fax: +49-931-70564-60

Abstract

The infrared-optical properties of ceramics are correlated with the complex index of refraction of the material and the structure of the ceramic [1, 2]. By changing these parameters, the infrared-optical properties can be changed in a relatively wide range.

The correlation of the structural properties, like the porosity or the pore sizes, and the material properties, like the complex index of refraction, on the one hand and the infrared-optical properties, like the emittance, on the other hand, are described by a solution of the equation of radiative transfer and the Mie-theory. Within this work, low-e ceramics, which have significantly lower emittances than conventional ceramics, were prepared by optimization of their composition and structure. The spectral emittance of these ceramics was measured, and from the spectral emittance a total emittance, which depends on temperature, was calculated. As a result one obtains ceramics, which have a total emittance of 0.2 at a temperature of 1100 K. In comparison to conventional ceramics with a typical total emittance of 0.8 at 1100 K, the use of such low-e ceramics will lead to a reduction in heat transfer via thermal radiation of about 70 %. For validation of the theory the results from our calculations were compared with experimentally obtained data.

Key words

Ceramics, emittance, infrared, low-e, scattering, three-flux approximation

1   Introduction

In many applications the heat transfer through materials and the heat exchange between the surfaces are important. In automotive applications ceramic coatings with low emittances are desirable. Hot parts, like the exhaust manifold or the catalytic converter can be covered with a ceramic coating. Such coatings should have a low emittance to reduce the heat transfer to neighboring parts within the engine compartment [3]. Additionally, ceramics with a low emittance are useful in any applications at high temperatures, where the heat exchange via radiation has to be suppressed. Beside ceramic coatings, monolithic ceramics with low-e properties are also highly interesting.

The total emittance of a ceramic depends on the temperature of this ceramic, as the spectral emittance varies with wavelength. In this work oxide ceramics are investigated, as they are white in the visible and the near infrared region. This means, that the emittance is relatively low for wavelengths below 2 µm. For opaque samples the emittance increases with

increasing wavelengths and becomes 1 at the so called Christiansen wavelength [4]. At the Christiansen wavelength the real part of the refractive index is 1, so that no reflection occurs. If the imaginary part of the refractive index is small compared to one, but non-vanishing and if the thickness of the sample is high enough, no transmittance occurs and all radiation is absorbed, i.e. the emittance becomes 1. For most oxide ceramics, the Christiansen wavelength lies between 8 µm and 16 µm. The Christiansen wavelength depends only on the refractive index of the material. Therefore no significant variation of the Christiansen wavelength can be achieved by changing the porosity or the structure of the ceramic.

But the shoulder, where the increase of the emittance appears, can be shifted towards higher wavelengths, by optimizing the porosity and structure of the ceramic. The Christiansen wavelength itself can be shifted towards higher wavelength by using materials with refractive indices, which are optimal. Therefore both parameters are varied in this work, the refractive index, by changing the material and the structure, by changing the parameters within the manufacturing process.

In this work monolithic samples were produced via a sintering process, as this is the most common method of producing ceramics. The results can also be applied to ceramic coatings, as such coatings can be produced in a similar way, for example via electrophoretic deposition with a sintering process afterwards.

2 Radiative transfer within porous media

The propagation of radiation through a porous medium like a ceramic is hindered by scattering and absorption. Scattering of radiation mainly occurs at the interface between the medium (for example the ceramic) and the surrounding medium (mostly air) and at the air-filled pores within the ceramic. The absorption mainly occurs within the ceramic. For reducing the emittance of a ceramic, the scattering has to be maximized and the absorption has to be minimized. The correlation between the scattering and absorption on the one hand and the complex refractive index $m = n + \mathrm{i} \cdot k$ and the structure of the medium on the other are discussed in the following chapters.

The propagation of radiation through a medium with known scattering and absorption coefficients can be described via the equation of radiative transfer. A solution of the equation of radiative transfer is presented in chapter 2.2. The scattering and absorption coefficients can be calculated from the known refractive index and the pore size distribution within the ceramic by using Mie-theory as explained in chapter 2.3. In chapter 2.1, the definitions of the spectral and total emittance are given.

2.1 Emittance

The emittance $\varepsilon_\lambda(T)$ of a surface at a given temperature is defined as the ratio of the intensity emitted by a surface $I_\lambda(T)$ and the intensity $I_{b,\lambda}(T)$ emitted by a black body at the same temperature T:

$$\varepsilon_\lambda = \frac{I_\lambda(T)}{I_{b,\lambda}(T)} \quad .$$

(1)

However, for semitransparent samples no emittance can be given, as the emittance of such ceramics is not only a surface property, but also a volumetric property. Additionally a temperature gradient may occur inside the ceramic. In such cases it is possible to use an apparent emittance, where the intensity $I_\lambda(T)$ in Eq. (1) represents the intensity emitted by

the ceramic sample with an average temperature T. For a simpler presentation in this paper, the apparent emittance is always called emittance.

The directional emittance ε_λ can be measured directly or calculated from the directional-hemispherical reflectance R_{dh} and transmittance T_{dh}:

$$\varepsilon_\lambda = 1 - R_{dh} - T_{dh} \quad . \tag{2}$$

The total emittance $\varepsilon(T)$ can be calculated from the spectral emittance ε_λ:

$$\varepsilon(T) = \frac{\int\limits_0^\infty \varepsilon_\lambda \cdot I_{b,\lambda}(T) \cdot d\lambda}{\int\limits_0^\infty I_{b,\lambda}(T) \cdot d\lambda} \quad . \tag{3}$$

The total emittance is a measure for the amount of energy, which is emitted by a sample at a certain temperature.

2.2 Equation of radiative transfer

The transmission of thermal radiation through semitransparent materials and the emission of radiation from semitransparent materials can be described by the equation of radiative transfer [5], which gives the variation of the spectral intensity I in dependence of the path x parallel to the radiation propagation within a plane-parallel sample:

$$\frac{dI(x)}{dx} = -E \cdot I(x) + \frac{S}{4\pi} \int\limits_{4\pi} I(x,\Omega') \cdot p(x,\Omega',\Omega) \cdot d\Omega' + A \cdot I_b(x) + E \cdot J(\tau) \quad , \tag{4}$$

with E: extinction coefficient, $E = A + S$, A: absorption coefficient, S: scattering coefficient, and $p(\Omega',\Omega)$: phase function for the radiation that is coming from the solid angle Ω' and is scattered into the solid angle Ω. The first term on the right hand side of Eq. (4) describes the exponential decrease of I caused by scattering and absorption events. The second and third term characterize the increase of I due to isotropic scattering and re-emission, respectively. The source term $J(\tau)$ accounts for the incoming radiation F, that reaches the point τ (optical depth, $\tau = E \cdot x$), if the sample is irradiated normal to the surface (Figure 1):

$$J(\tau) = \frac{\omega_0 \cdot F}{4 \cdot \pi} \cdot \rho_p(\tau) = \frac{\omega_0 \cdot F}{4 \cdot \pi} \cdot \frac{1 - R_p}{1 - R_p^2 \cdot \exp(-2 \cdot \tau_0)} \left[\exp(-\tau) + R_p \cdot \exp(-2 \cdot \tau_0 + \tau)\right] \quad , \tag{5}$$

with

$$R_p(n,k) = \frac{(n-1)^2 + k^2}{(n+1)^2 + k^2} \quad , \tag{6}$$

3

being the directional-directional reflectance normal to the surface air – medium and medium – air and $\rho_p(\tau)$ being the internal reflectance, which is given as the sum of the terms in Figure 1.
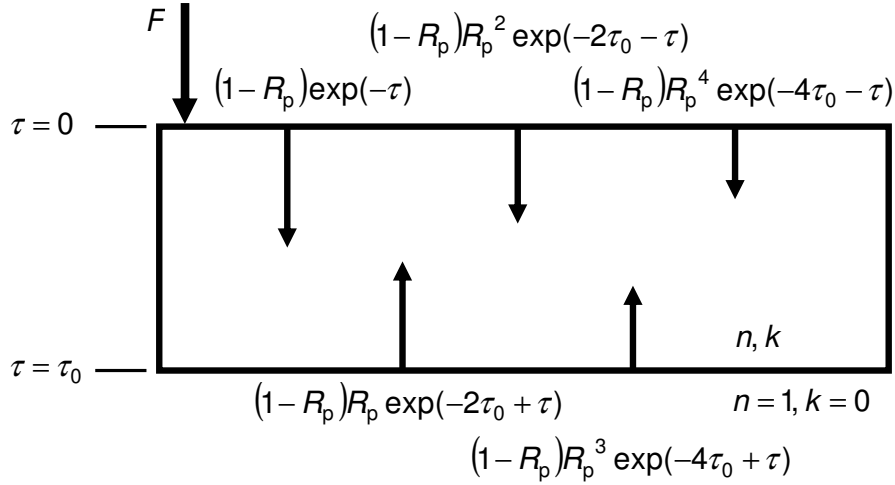

Figure 1: Multiple reflections of the incoming radiation F, which is impinging normal to the sample surface. Also given are the reflected parts of the incoming radiation. Summarizing these terms leads to the internal reflectance $\rho_p(\tau)$.

Eq. (4) can be rewritten and simplified for isotropic scattering ($p \equiv 1$):

$$\mu \cdot \frac{dI(\tau)}{d\tau} = -I(\tau) + \frac{\omega_0}{2} \int_{-1}^{1} I(\tau, \mu') \cdot d\mu' + \frac{A}{E} \cdot \frac{n^2 \cdot \sigma \cdot T^4(\tau)}{\pi} + J(\tau) \quad , \tag{7}$$

with τ: optical depth, $\tau = E \cdot x$, ω_0: albedo, $\omega_0 = S/E$, μ: direction cosine, $\mu = \cos\theta$, and θ: scattering angle.

The equation of radiative transfer can be solved for isotropic scattering. The transformation of the solution to anisotropic scattering can be made via a scaling concept [6]. In this scaling concept an effective optical thickness τ_0^* and an effective albedo ω_0^* are defined, which are correlated to the optical thickness $\tau_0 = E \cdot d$ and the albedo ω_0 by the anisotropy factor g:

$$\tau_0^* = \tau_0 \cdot (1 - \omega_0 g) \quad \text{and} \quad \omega_0^* = \frac{\omega_0 \cdot (1-g)}{1 - \omega_0 \cdot g} \quad , \tag{8}$$

with

$$g = \int_{4\pi} \cos\theta \cdot p(\theta) \cdot d\Omega \quad . \tag{9}$$

The values of the anisotropy factor are within the interval −1 (backward scattering) to +1 (delta function like forward scattering). The effective extinction coefficient E^* is defined analogously (see also Eq. (24)).

To solve Eq. (7) the discrete ordinate approximation can be used [7]. For this approximation the integral in Eq. (7) is transformed into a sum over a few intensities. For the three-flux approximation three discrete directions are regarded:

4

$$\int_{-1}^{1} I(\tau^*, \mu') \cdot d\mu' \quad \rightarrow \quad \sum_{j=-1}^{1} a_j \cdot I_j \quad . \tag{10}$$

The direction cosine of these directions are determined from the weight factors a_j of the intensities I_j to [7]:

$$\mu_{-1} = -\frac{2}{3} \quad , \quad \mu_0 = 0 \quad , \quad \mu_1 = \frac{2}{3} \quad . \tag{11}$$

The boundary conditions are

$$I_1(\tau^* = 0) = \overline{R_i} \cdot I_{-1}(\tau^* = 0) \quad , \tag{12}$$

$$I_{-1}(\tau^* = \tau_0{}^*) = \overline{R_i} \cdot I_1(\tau^* = \tau_0{}^*) \quad . \tag{13}$$

The mean internal reflectance $\overline{R_i}$ can be determined from the angular dependent reflectance R_i:

$$\overline{R_i}(n,k) = \frac{\int_0^1 \mu \cdot R_i(\mu, n, k) \cdot d\mu}{\int_0^1 \mu \cdot d\mu} = 2 \cdot \int_0^1 \mu \cdot R_i(\mu, n, k) \cdot d\mu \quad . \tag{14}$$

It represents that part of the scattered radiation, which hits the interface medium – air from all directions and is reflected back into the medium.

The three-flux approximation has mathematically the same complexity as the two-flux approximation, but provides a far better accuracy [8].

Finally one gets the macroscopic values directional-hemispherical reflectance R_{dh} and transmittance T_{dh} in dependence on the microscopic values effective extinction coefficient E^*, effective albedo ω_0^* and the complex refractive index $m = n + i \cdot k$ of the medium:

$$T_{dh} = \frac{\left(1 - \overline{R_i}\right) \cdot I_{+1}(\tau^* = \tau_0{}^*, \omega_0{}^*) + \dfrac{F}{\pi} \cdot \dfrac{\left(1 - R_p\right)^2}{1 - R_p{}^2 \cdot \exp(-2\tau_0{}^*)} \cdot \exp(-\tau_0{}^*)}{\dfrac{F}{\pi}} \quad , \tag{15}$$

$$R_{dh} = \frac{\left(1 - \overline{R_i}\right) \cdot I_{-1}(\tau^* = 0, \omega_0{}^*) + \dfrac{F}{\pi} \cdot R_p + \dfrac{F}{\pi} \cdot \dfrac{\left(1 - R_p\right)^2 \cdot R_p \cdot \exp(-2\tau_0{}^*)}{1 - R_p{}^2 \cdot \exp(-2\tau_0{}^*)}}{\dfrac{F}{\pi}} \quad . \tag{16}$$

When measuring the reflectance and transmittance of the sample, the reemission term in Eq. (4) can be neglected, as the incoming radiation is modulated by FTIR-technique, whereas the emitted radiation is not modulated. For calculating the emitted radiation of the sample as a function of the sample temperature, the boundary conditions have to be modified and the source term in Eq. (4) can be neglected, as no incoming radiation has to be considered.

2.3 Mie-theory

Mie-theory gives a description of the scattering of an electromagnetic plane wave at a spherical particle. This theory is named after Gustav Mie, who first published it in 1908 [9]. For spheres, the Maxwell equations can be solved exactly. The whole procedure is described in detail in [10, 11, 12]. As a result of this calculations one gets the so called development coefficients a_j und b_j, which are determined by the Ricatti-Bessel functions ψ_j, ζ_j and their derivatives ψ'_j, ζ'_j [11]:

$$a_j = \frac{\psi'_j(m_{air} z)\psi_j(mz) - \dfrac{m_{air}}{m}\psi_j(m_{air} z)\psi'_j(mz)}{\psi'_j(m_{air} z)\zeta_j(mz) - \dfrac{m_{air}}{m}\psi_j(m_{air} z)\zeta'_j(mz)} \quad , \tag{17}$$

$$b_j = \frac{\dfrac{m_{air}}{m}\psi'_j(m_{air} z)\psi_j(mz) - \psi_j(m_{air} z)\psi'_j(mz)}{\dfrac{m_{air}}{m}\psi'_j(m_{air} z)\zeta_j(mz) - \psi_j(m_{air} z)\zeta'_j(mz)} \quad . \tag{18}$$

m_{air} gives the complex refractive index of the pores, which are filled with air and m gives the complex refractive index of the solid ceramic. The Ricatti-Bessel functions ψ_j and ζ_j are defined by the spherical Bessel and Hankel functions j_j and h_j [10]:

$$\psi_j(v) = v \cdot j_j(v) \quad , \quad \zeta_j(v) = v \cdot h_j^{(1)}(v) \quad . \tag{19}$$

The definitions of the spherical Bessel and Hankel functions are for example given in [13]. Finally one gets the absorption and scattering coefficients of spheres as a function of the complex refractive indices m_{air}, m and the size parameter z:

$$z = \frac{\pi \cdot D}{\lambda} \quad , \tag{20}$$

where D is the particle diameter and λ is the wavelength of the incoming radiation. The Mie-theory is only valid for spherical particles, but even for non-spherical particles reliable results, as mentioned in literature [10], can be obtained.

In porous ceramics mainly the air-filled pores, which are embedded in the solid ceramic with its complex refractive index m, are responsible for the scattering of radiation.

The scattering cross section C_{sca} and the absorption cross section C_{abs} are defined as the quotient of the scattered or absorbed radiant power and the incoming intensity, respectively. By dividing the scattering and absorption cross sections by the geometrical cross section, one gets the efficiency for scattering Q_{sca} and absorption Q_{abs}, which are determined by the development coefficients a_j and b_j [11]:

$$Q_{sca} = \frac{C_{sca}}{\pi \left(\frac{D}{2}\right)^2} = \frac{2}{z^2} \sum_{j=1}^{\infty} (2j+1)\left(|a_j|^2 + |b_j|^2\right)$$

$$Q_{ext} = \frac{C_{abs}}{\pi \left(\frac{D}{2}\right)^2} = \frac{2}{z^2} \sum_{j=1}^{\infty} (2j+1)\mathrm{Re}\left(a_j + b_j\right) \qquad .$$

(21)

$$Q_{abs} = Q_{ext} - Q_{sca}$$

The efficiency for extinction Q_{ext} is defined as the sum of the efficiency for scattering and absorption. With the known porosity Π of the sample, the extinction coefficient E and the scattering coefficient S can be calculated for a given pore diameter D [14]:

$$E(\lambda) = \frac{3}{2} \Pi \frac{Q_{ext}(\lambda)}{D} \quad , \quad S(\lambda) = \frac{3}{2} \Pi \frac{Q_{sca}(\lambda)}{D} \qquad .$$

(22)

The anisotropy factor g is determined by the development coefficients a_j and b_j, too [15]:

$$g = \frac{4}{z^2 Q_{ext}} \sum_{j=1}^{\infty} \left[\frac{j(j+2)}{j+1} \mathrm{Re}\left(a_j \bar{a}_{j+1} + b_j \bar{b}_{j+1}\right) + \frac{2j+1}{j(j+1)} \mathrm{Re}\left(a_j \bar{b}_j\right) \right] \quad .$$

(23)

With the anisotropy factor, the effective efficiency for extinction Q_{ext}^* and scattering Q_{sca}^* can be derived as well as the effective extinction and scattering coefficients E^* and S^*:

$$Q_{ext}^* = Q_{ext}(1 - \omega_0 g) \quad , \quad E^* = E(1 - \omega_0 g)$$

$$Q_{sca}^* = Q_{sca}(1 - g) \quad , \quad S^* = S(1 - g)$$

(24)

The scattering within a powder occurs at the powder-particles, that means at the interfaces air-medium, whereas the scattering inside a ceramic occurs at the air-filled pores, that means at the interfaces medium-air (Figure 2), as mentioned above. Both cases can be described with Mie-theory, only the refractive indices need to be changed.
Normally one has not only pores with a given diameter D, but a pore size distribution. Often one assumes that the pore volume within a logarithmic diameter interval $\Delta \ln D$ is distributed like a logarithmic normal distribution [11]:

$$f(D)\Delta \ln D = \frac{1}{\sqrt{2\pi}\sigma_g} \exp\left[-\frac{(\ln D - \ln D_M)^2}{2\sigma_g^2} \right] \Delta \ln D \quad .$$

(25)

By a least-squares-fit with the measured spectral effective extinction coefficient E^*_{exp} and the spectral effective extinction coefficient E^* calculated from Eq. (22) and Eq. (24), the modal value D_M and the geometric mean standard deviation σ_g can be calculated.
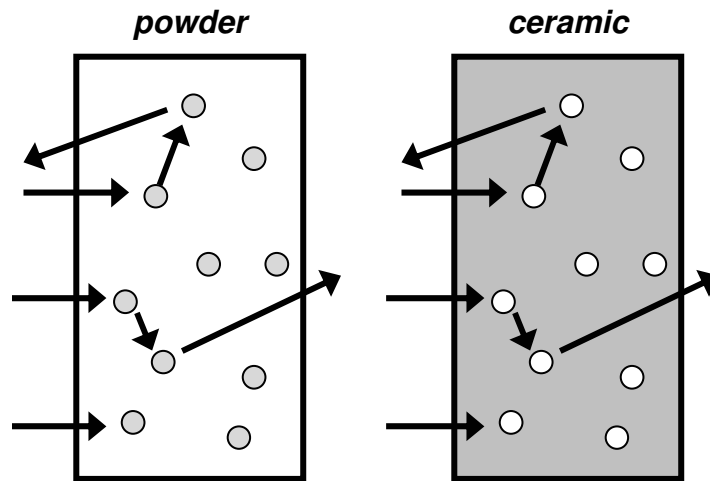
Figure 2: Within a powder scattering occurs mainly at the powder-particles (shown on the left side), whereas inside a ceramic scattering occurs mainly at the air-filled pores (shown on the right side).

3 Sample production and experimental set up

The monolithic samples, which are characterized in this work, were made via a sintering process at ZAE Bayern. First, the ceramic powders were pressed at 100 MPa. Then the obtained green bodies were sintered at different temperatures and with different sintering times. The porosities of the samples were measured using the Archimedes principle. The resulting data of the produced sample slides, which have a diameter of about 30 mm, can be seen in Table 1. Additionally several SEM (scanning electron microscope) – pictures of the samples were made.

Table 1: Datasheet of the monolithic ceramic samples, prepared at ZAE Bayern. The samples have a diameter of about 30 mm.

sample No.	material	thickness d / mm	sintering temperature T_s / K	sintering time t_s / h	porosity Π
1	HfO_2	1.3	1473	1	0.39
2	Al_2O_3	4.0	1973	8	0.02
3	Al_2O_3	3.7	1873	6	0.27
4	TiO_2	1.3	1873	8	0.01
5	TiO_2	2.3	1373	6	0.42
6	Y_2O_3	2.1	1873	6	0.17
7	Y_2O_3	2.4	1773	2	0.37

The ceramic coating presented in this work was prepared at the German Aerospace Center (DLR) via EB-PVD (electron-beam physical-vapor deposition) as explained in [16].
The directional-hemispherical transmittance T_{dh} of both, the ballistic transmitted radiation and the diffusely scattered radiation at the backside of the sample was measured by an integrating sphere (Figure 3) [17]. The directional-hemispherical reflectance R_{dh} can also be measured using an integrating sphere. For the wavelength range from 0.25 µm to

2.5 µm a Perkin Elmer lambda 9 diffraction-spectrometer was used and for the wavelength range from 1.4 µm to 18 µm a Bruker IFS 66v FTIR-spectrometer was used.
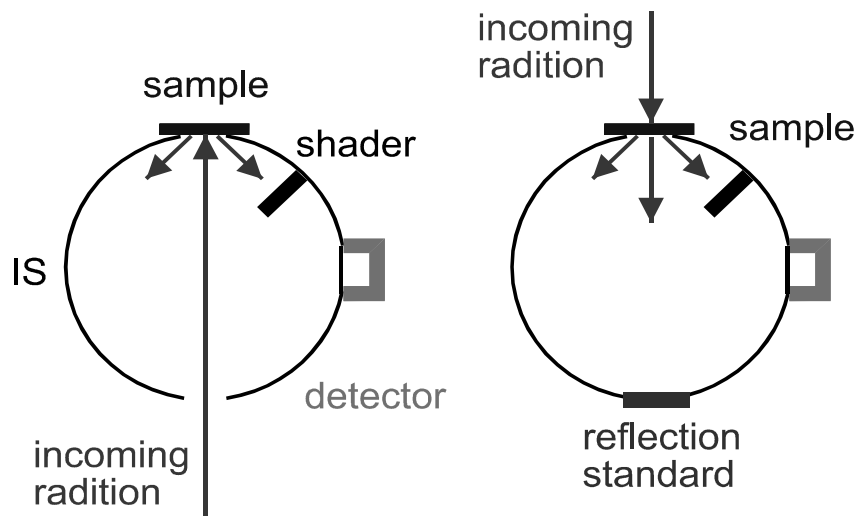

Figure 3: Measurement set-ups (directional-hemispherical reflectance on the left side and directional-hemispherical transmittance on the right side) with an integrating sphere (IS). The internal surface of the integrating sphere is coated with a highly reflecting coating, which reflects the radiation diffusely.

4   Results and analysis

The real part n and the imaginary part k of the complex refractive index m of the materials investigated in this work are depicted in Figure 4 and Figure 5, respectively. The data was taken from literature [18, 19] to be used in the calculations described above.
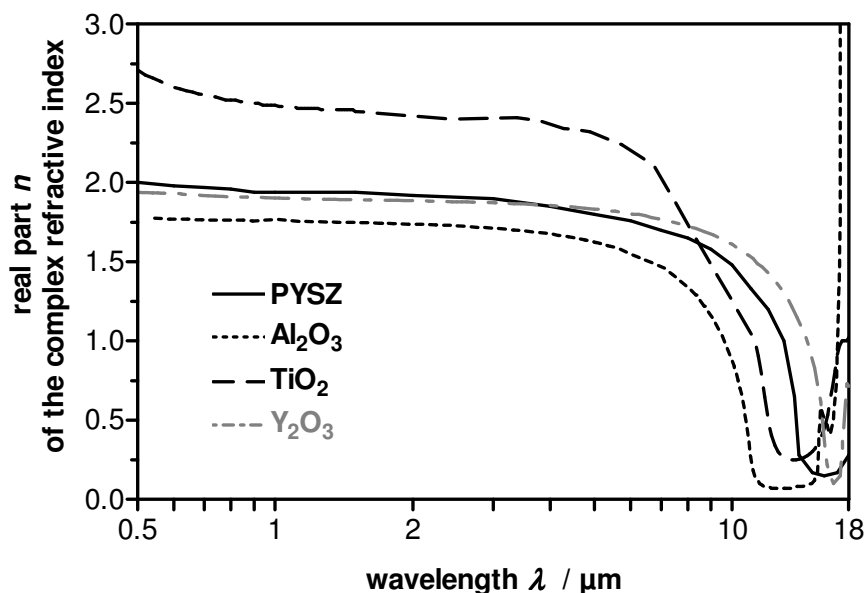

Figure 4: Real part n of the complex refractive index of several ceramics in dependence on the wavelength λ from 0.5 µm to 18 µm at ambient temperature.
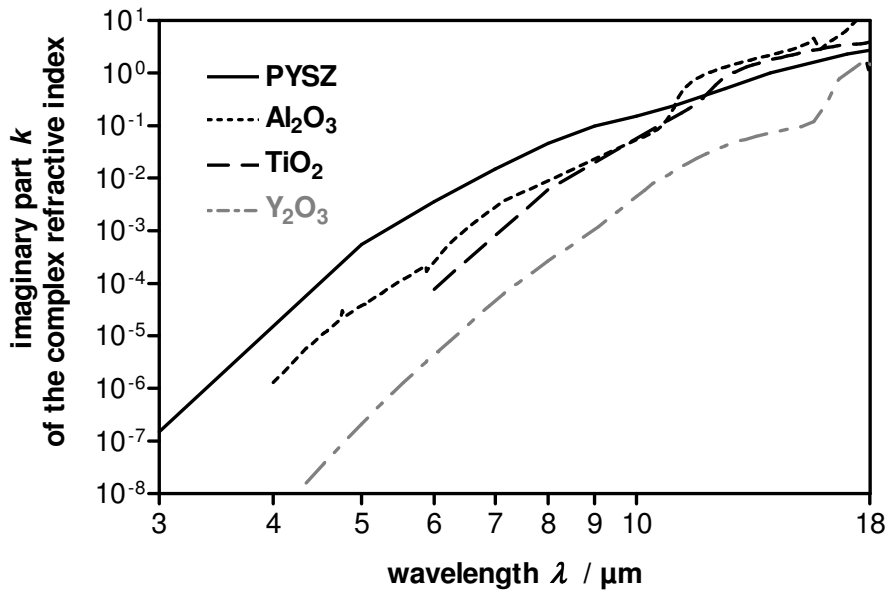
Figure 5: Imaginary part k of the complex refractive index of several ceramics in dependence on the wavelength λ from 3 µm to 18 µm at ambient temperature, note the logarithmic ordinate.

The directional-hemispherical reflectance R_{dh} and transmittance T_{dh} of the samples were measured. Samples with different thicknesses were produced. For the determination of the emittance, samples with a vanishing transmittance were produced. Additionally samples with a non-vanishing transmittance were made, for an analysis of the structure.

First, the emittance was determined from the samples with vanishing transmittance. The emittance of conventional coatings, like thermal barrier coating, made of PYSZ (partially yttria stabilized zirconia), is relatively high. The spectral emittance of one PYSZ-coating is depicted in Figure 6. The total emittance at 1100 K is 0.8. The spectral emittance of hafnium oxide (a conventional monolithic ceramic), also depicted in Figure 6, has a total emittance of 0.73, which is only slightly smaller. Hafnium oxide is not often used, but it is similar to zirconia, as it has almost the same properties as zirconia, which is used in a wide range of applications.

Both ceramics show, like most oxide ceramics, a low emittance in the visible wavelength region. Therefore, they appear white. But with increasing wavelength, the emittance increases and becomes one at the so called Christiansen wavelength. For PYSZ and hafnium oxide, the Christiansen wavelength lies at 13 µm, independent of the structure.
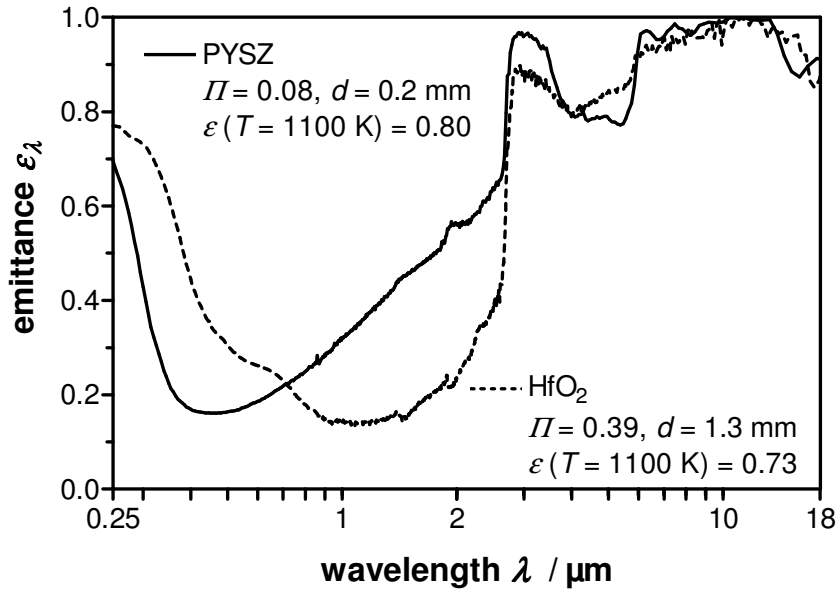
Figure 6: Directional emittance ε_λ of partially yttria stabilized zirconia (PYSZ) and hafnium oxide in dependence on the wavelength λ from 0.25 µm to 18 µm at ambient temperature.

By changing the structure it is possible to shift the slope of the emittance towards longer wavelength. This is demonstrated in Figure 7 for alumina. The total emittance at 1100 K of a sample with a porosity of 0.02 is 0.53. By increasing the porosity, the total emittance can be decreased to 0.24. This is due to the fact, that the spectral emittance is reduced, especially between 2 µm and 8 µm.

Due to a higher imaginary part of the refractive index, the same procedure does not lead to a significant reduction of the spectral emittance of hafnium oxide, although the Christiansen wavelength of alumina lies at 10 µm and is therefore lower than the Christiansen wavelength of hafnium oxide. As a consequence, both parameters need to be optimized, the material with its refractive index and the structure of the material.
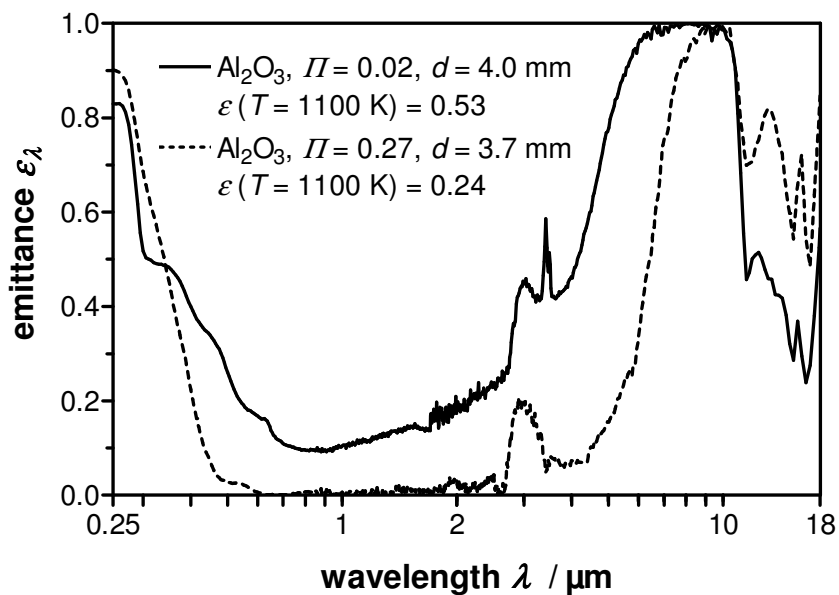

Figure 7: Directional emittance ε_λ of alumina in dependence on the wavelength λ from 0.25 µm to 18 µm at ambient temperature.

TiO_2 has with 12 µm a higher Christiansen wavelength than Al_2O_3 and a higher refractive index than HfO_2 and ZrO_2. Therefore, the total emittance at 1100 K is lower than for the named materials. The spectral emittance for two TiO_2-samples is depicted in Figure 8. The resulting total emittance at 1100 K is 0.34 for a porosity of 0.01 and 0.27 for a porosity of 0.42.
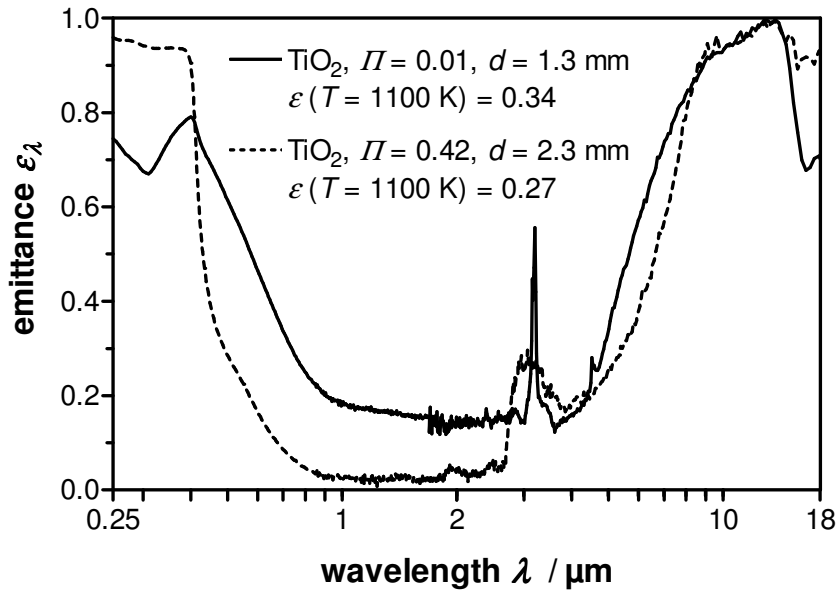

Figure 8: Directional emittance ε_λ of titania in dependence on the wavelength λ from 0.25 µm to 18 µm at ambient temperature.

In Figure 9, the spectral emittance of yttria is plotted for different porosities. The Christiansen wavelength lies at 15 µm. Because of that and the fact, that yttria has the lowest imaginary part of the investigated materials, the emittance at 1100 K is lower than for the other ceramics characterized in this work. The emittance can be reduced additionally by varying the structure. For a porosity of 0.17 one gets an emittance of 0.19 at 1100 K. If the porosity is increased furthermore, the total emittance also increases. Therefore an optimum of the structure and porosity exists, at which the total emittance has a minimum.
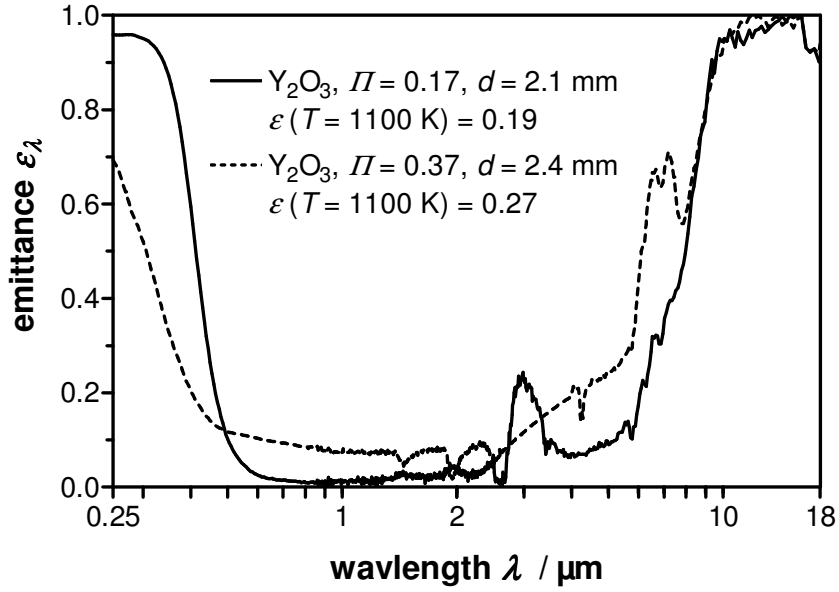
Figure 9: Directional emittance ε_λ of yttria in dependence on the wavelength λ from 0.25 µm to 18 µm at ambient temperature.

The Christiansen wavelength and the total emittance at 1100 K for all samples are shown in Table 2.

Table 2: Christiansen wavelength λ_{Chr} and total emittance $\varepsilon(T)$ of the measured monolithic ceramic samples.

sample No.	material	Christiansen wavelength λ_{Chr} / µm	total emittance $\varepsilon(T)$ at $T = 1100$ K
1	HfO_2	13	0.73
2	Al_2O_3	10	0.53
3	Al_2O_3	10	0.24
4	TiO_2	12	0.34
5	TiO_2	12	0.27
6	Y_2O_3	15	0.19
7	Y_2O_3	15	0.27

To get a correlation between the structure and the total emittance, SEM (scanning electron microscope) – pictures of the samples were taken. In Figure 10, Figure 11 and Figure 12, SEM-pictures of the samples 4, 5 and 6 are shown, respectively. The porosity of sample 4 (TiO_2) is very low ($\Pi = 0.01$), therefore, the dimensions of the structure are about 50 µm. Due to the relatively high real part of the refractive index, a total emittance of 0.34 results at 1100 K. With a lower sintering temperature and time, one gets a significantly higher porosity ($\Pi = 0.42$) with a finer structure (sample 5) and dimensions of about 3 µm. This results in a lower total emittance of 0.27. Sample 6 (Y_2O_3 with $\Pi = 0.17$) has a structure with dimensions of about 1 µm and a total emittance of 0.19. This is due to the structural properties and the Christiansen wavelength, which lies at a longer wavelength, compared to TiO_2.
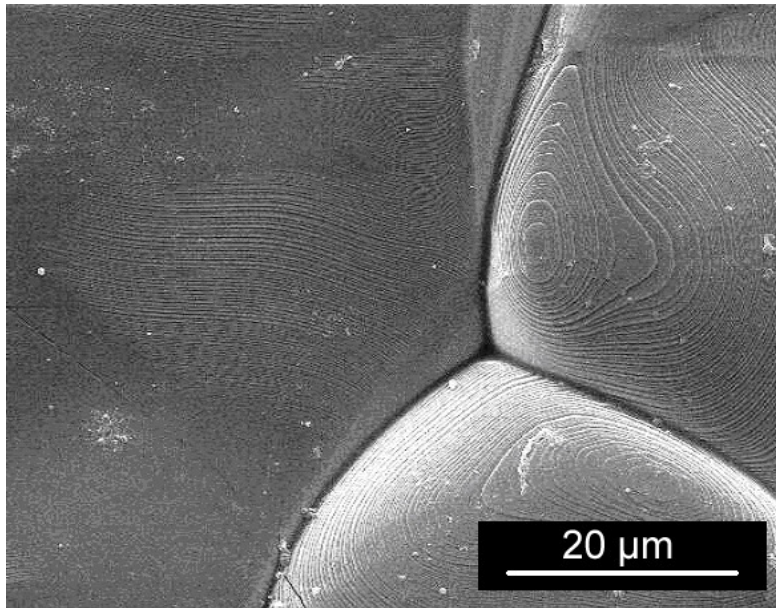
Figure 10: SEM-picture (enlargement factor = 2000) taken from sample 4 (TiO$_2$ with $\Pi = 0.01$).
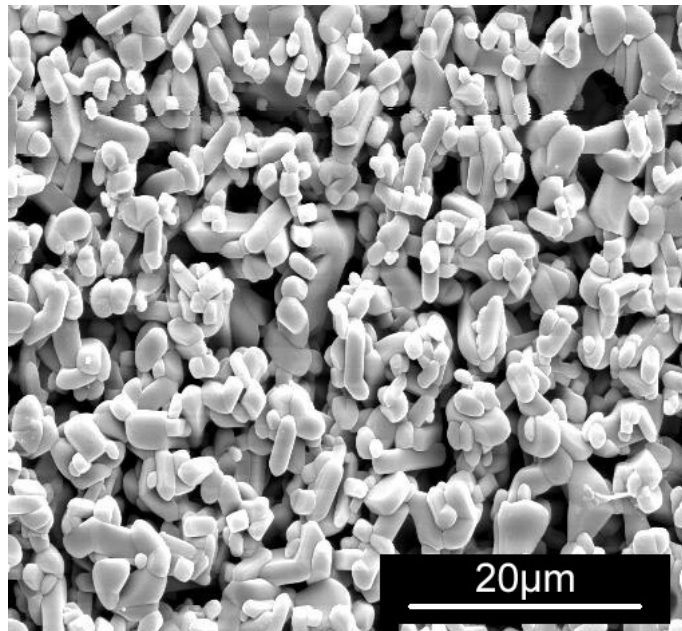

Figure 11: SEM-picture (enlargement factor = 2000) taken from sample 5 (TiO$_2$ with $\Pi = 0.42$).
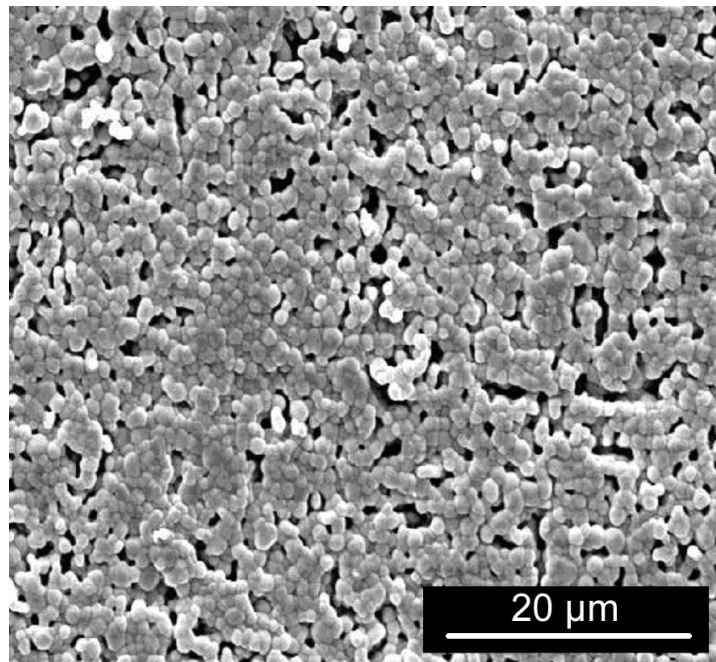
Figure 12: SEM-picture (enlargement factor = 2000) taken from sample 6 (Y_2O_3 with $\Pi = 0.17$).

To get more information about the structure of sample 6, the directional-hemispherical reflectance and transmittance were measured for a thinner sample, which was prepared and sintered together with sample 6, so that both samples have the same properties, except for the thickness.

The effective optical thickness and the effective albedo, which are equivalent to the effective extinction coefficient and effective scattering coefficient, are determined using Eq. (15) and Eq. (16). From the known effective scattering coefficient the dimensions of the structure (Eq. (25)) were calculated using Mie-theory. The resulting structural properties are depicted in Figure 13. Although spherical pores were assumed as scattering centers, the resulting dimensions agree well with the SEM-pictures. Because of this, the pore volume distribution in Figure 13 gives the distribution of the structural dimensions.
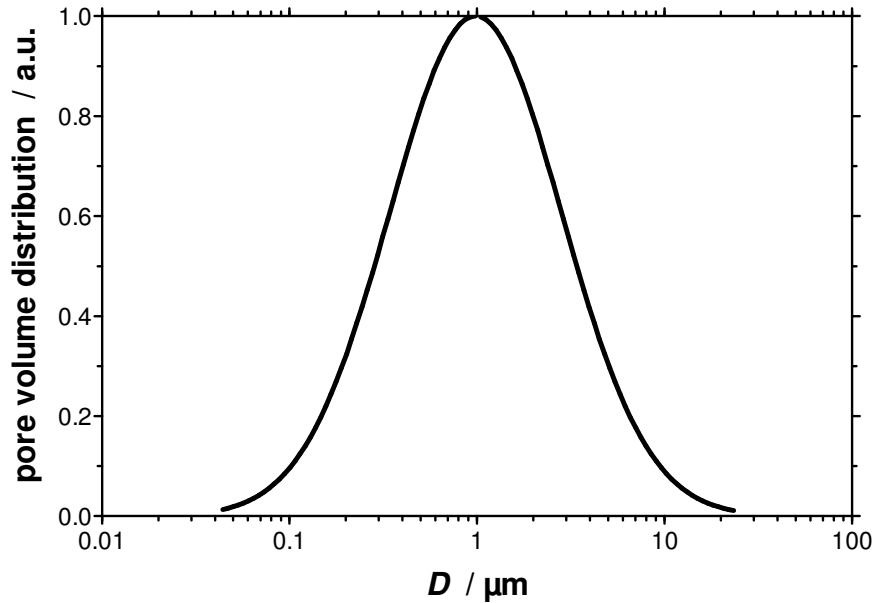
Figure 13: Pore volume distribution of sample 6 (Y$_2$O$_3$ with Π = 0.17) determined via scattering of radiation inside the ceramic.

5 Conclusions

It was shown, that the infrared-optical properties of oxide ceramics can be varied in a relatively wide range, by varying the material and the structure of the sample. Some of the most promising materials were investigated in this work. As a result the emittance was reduced from 0.80 to 0.19 by optimizing the manufacturing process. One requirement for lowering the emittance is the usage of a material with a high real part and a low imaginary part of the complex refractive index. A second requirement is the optimal structure of the produced sample. The dimensions of the structure should have the same order of magnitude or be slightly smaller, than the wavelength of the incoming radiation, to get a maximal reflectance and therefore a minimal emittance.

In this work preliminary investigations were done to check the potential of possible reductions of the emittance of ceramics. As these investigations were successful, work is planned for a further reduction of the emittance, e.g. an emittance below 0.1 at 1100 K. In the future, mixtures of different materials with variation of the structure will be investigated. For example, a mixture of titania and yttria, would be promising, as it unites the high real part of the refractive index of titania with the low imaginary part of the refractive index of yttria. As the refractive index of mixtures can differ significantly from the refractive index of the raw material a detailed analysis of the mixtures will be necessary.

16

7 Symbols

μ	direction cosine	
τ	optical depth	
τ_0	optical thickness	
Π	porosity	
θ	scattering angle	rad
ε	total emittance	
ε_λ	spectral emittance	
λ	wavelength	m
λ_{Chr}	Christiansen wavelength	m
Ω, Ω'	solid angle	sr
ω_0	albedo	
σ_g	geometric mean standard deviation	
ψ_j, ζ_j	Ricatti-Bessel functions	
ρ_p	internal reflectance	
A	absorption coefficient	m^{-1}
a_i	weight factors	
a_j, b_j	development coefficients	
C_{abs}	absorption cross section	m^2
C_{ext}	extinction cross section	m^2
C_{sca}	scattering cross section	m^2
d	thickness	m
D	diameter	m
D_M	modal value	m
E	extinction coefficient	m^{-1}
F	radiative flux	W m^{-1} m^{-2}
g	anisotropy factor	
I_λ	spectral intensity	W m^{-1} m^{-2} sr^{-1}
$I_{b,\lambda}$	spectral intensity of a black body	W m^{-1} m^{-2} sr^{-1}
J	source term	W m^{-1} m^{-2} sr^{-1}
k	imaginary part of the complex refractive index	
m	complex refractive index	
n	real part of the complex refractive index	
p	phase function	
Q_{abs}	efficiency for absorption	
Q_{ext}	efficiency for extinction	
Q_{sca}	efficiency for scattering	
R_{dh}	directional-hemispherical reflectance	
R_i	angular dependent reflectance	
$\overline{R_i}$	mean internal reflectance	
R_p	reflection of perpendicular beam onto surface	
S	scattering coefficient	m^{-1}
T	temperature	K
T_{dh}	directional-hemispherical transmittance	
t_s	sintering time	s
T_s	sintering temperature	K
x	length	m
z	size parameter	

Subscript: * effective

8 References

[1] J. Manara, R. Caps, F. Raether, J. Fricke, *Optics Communications* 168 (1999) 237-250

[2] J. Manara, R. Caps, J. Fricke, *International Journal of Thermophysics* **26** (2005) 531-542

[3] A. Knote, H.G. Krüger, H. Kern, J. Manara, *Presentation at the "Thüringer Werkstoff-tag 2004"*

[4] J. Manara, Infrarot-optischer Strahlungstransport zur Analyse der Struktur und der Wärmeleitfähigkeit von Keramiken für Hochtemperaturanwendungen (Würzburg: Dissertation zur Erlangung des naturwissenschaftlichen Doktorgrades der Bayerischen Julius-Maximilians- Universität Würzburg, 2001)

[5] T. Burger, J. Kuhn, R. Caps, J. Fricke, *Applied Spectroscopy* **51** (1997) 309-319

[6] B.H.J. McKellar, M.A. Box, *Journal of Atmospherical Science* **38** (1981) 1063-1068

[7] M.G. Kaganer, *Optica und Spectroscopica* **26** (1969) 443-456

[8] S. Chandrasekhar, *Radiative Transfer* (New York: Dover Publications Inc., 1960)

[9] G. Mie, *Annalen der Physik* **25** (1908) 377-445

[10] C.F. Bohren, D.R. Huffmann, *Absorption and Scattering of Light by Small Particles* (New York: John Wiley & Sons, 1983)

[11] M. Kerker, *The Scattering of Light and Other Electromagnetic Radiation* (Orlando: Academic Press, 1969)

[12] H.C. van de Hulst, *Light Scattering by Small Particles* (New York: Dover Publications Inc., 1981)

[13] G. Berendt, E. Weimar, *Mathematik für Physiker, Band 2: Funktionentheorie, gewöhnliche und partielle Differentialgleichungen* (Weinheim: VCH Verlagsgesellschaft mbH, 1990)

[14] R. Caps, *Strahlungsströme in evakuierten thermischen Superisolationen* (Würzburg: Dissertation zur Erlangung des naturwissenschaftlichen Doktorgrades der Bayerischen Julius-Maximilians- Universität Würzburg, 1985)

[15] H.C. Hottel, A.F. Sarofim, *Radiative Transfer* (New York: McGraw-Hill, 1967)

[16] J. Manara, R. Brandt, J. Kuhn, J. Fricke, T. Krell, U. Schulz, M. Peters, W:A: Kaysser, *High Temp. – High Press.* **32** (2000) 361-368

[17] T. Burger, J. Fricke, J. Kuhn, *Near Infrared Spectrosc.* **6** (1998) 33-40

[18] E.D. Palik, *Handbook of Optical Constants of Solids* (San Diego: Academic Press, 1998)

[19] H. Tanaka, S. Sawai, K. Morimoto, K. Hisano, *Journal of Thermal Analysis and Calorimetriy* **64** (2001) 867-872